Performance Engineering and Topological Design of Metro WDM Optical Networks Using Computer Simulation

Neophytos Antoniades, *Member, IEEE*, Aleksandra Boskovic, Ioannis Tomkos, Nicholas Madamopoulos, *Member, IEEE*, Mirim Lee, *Member, IEEE*, Ioannis Roudas, David Pastel, Manish Sharma, and Michael J. Yadlowsky

***Abstract*—This paper demonstrates the use of computer simulation for topological design and performance engineering of transparent wavelength-division multiplexing metropolitan-area networks. Engineering of these networks involves the study of various transport-layer impairments such as amplifier noise, component ripple, chirp/dispersion, optical crosstalk, waveform distortion due to filter concatenation, fiber nonlinearities, and polarization effects. A computer simulation methodology composed of three main simulation steps is derived and implemented. This methodology obtains performance estimations by applying efficient wavelength-domain simulations on the entire network topology, followed by time-/frequency-domain simulations on selected paths of the network and finally Q-budgeting on an identified worst case path. The above technique provides an efficient tool for topological design and network performance engineering. Accurate simulation models are presented for each of the performance impairments, and the computer simulation methodology is used for the design and engineering of a number of actual metro network architectures.**

***Index Terms*—Computer simulation, optical networks, Q-budgeting, transport layer impairments, WDM.**

I. Introduction

THE tremendous growth in broadband communication services, brought about by the phenomenal expansion of the Internet, has triggered an unprecedented demand for bandwidth in telecommunication networks. Multiwavelength fiber-optic technology appeared as the solution for the bandwidth-hungry applications of the mid- to late 1990s, mainly due to its potential for nearly unlimited transparent capacity and extensive bandwdith management functionalities [1]. More bandwidth than ever before can now be used for long-haul transport and service provisioning, as fiber installations and wavelength-division multiplexing (WDM) equipment increased the capacity and lowered the cost per bit for these networks. Unfortunately, the metropolitan-area network environment has lagged behind in the availability of low-cost fast service provisioning using WDM. One of the main reasons has been the legacy infrastructure of synchronous optical network/synchronous digital hierarchy (SONET/SDH) equipment in metro regions. Until recently, most of the network functionality (e.g., signal add/drop, performance monitoring, and cross-connecting) has been provided electronically, which resulted in extensive optical-to-electronic and electronic-to-optical conversions (O-E-O) at each node in the network (opaque network designs). In contrast to long-haul optical networks, which are optimized for transmitting very high bit rates over long distances with very few add/drops, metro networks should be optimized to offer flexible connections and scalable bandwidth for new services on the optical layer. Since traffic requirements in this environment can change constantly [2], it is important to have the right technology to deal with possible network reconfigurations and varying network loads. The presence of multiple customers in the metro environment having diverse requirements makes the traditional opaque network designs (O-E-O) difficult to scale and adapt in a cost-effective way. Unlike long-haul networks, the metro networks of today are driven by central office access and transmission equipment costs, which are shared among a significantly smaller revenue base. New metro-area equipment must offer significantly increased functionality and performance at a lower cost per connection. It is only lately that the WDM technology and the optical transparency it allows have matured enough and become sufficiently cost effective to replace the traditional transponder-based designs in metro. Transparent WDM networks offer service flexibility based on support for different bit rates, modulation formats, and data types. Reconfigurability extends this by enabling efficient sharing of resources and service upgrades. Optical components are now used to route wavelengths transparently (no O-E-Os in the optical path) through the network (wavelength-routed designs), reducing cost and providing extensive flexibility in combining different protocols and bit rates. It must be noted that WDM does not preclude the use of SONET/SDH functionalities, which can now be offered on a wavelength-by-wavelength basis. The last two years have marked the introduction of WDM in metro applications through work on architectural proof-of-concept, experimental demonstrations, field trials, and finally real commercial deployments [3]–[9]. However, to our knowledge, there has been no in-depth published study on designing and engineering specific transparent metro network WDM architectures.

In this paper, we investigate the feasibility of transparent metropolitan-area networks and successfully demonstrate

Manuscript received February 14, 2001; revised July 14, 2001.

N. Antoniades, A. Boskovic, I. Tomkos, N. Madamopoulos, M. Lee, I. Roudas, and M. Sharma are with the Photonics Research and Test Center, Corning Inc., Somerset, NJ 08873 USA (e-mail: antoniadna@corning.com).

D. Pastel and M. J. Yadlowsky are with the Optical Networking Devices Division, Corning Inc., Corning, NY 14831 USA.

Publisher Item Identifier S 0733-8716(02)00151-8.

how to use computer transport-layer simulation for performance engineering and topology design focusing on specific network architectures. Engineering these networks from a transport-layer point of view can become a rather complex task. Distances over which optical signals travel in sections of these networks can potentially be less than 80 km, so optical amplification may not be needed. In these cases, channel optical power may not be adequate and receiver electrical noise can become a performance issue. For designs that do use optical amplifiers, amplified spontaneous emission (ASE) noise and signal power divergence can become important performance issues. The latter is the difference in power among the strongest and the weakest channels and can be the result of a number of effects, most importantly, component insertion loss variation along the wavelength plan, amplifier gain spectrum variations, imperfections on the performance of the gain flattening filters or multiplexer/demultiplexer (MUX/DMUX) filters, polarization-dependent loss (PDL), and fiber loss variations along the channel plan. Signal power divergence can result in significant performance degradations in a network. To mitigate its effects, we demonstrate the need for power equalization as essential for guaranteeing network performance.

Dispersion/chirp-induced waveform distortion is another effect that the network designer needs to consider. The choice of the optical transmitter and its associated characteristics will determine the maximum distance that the signal can be transmitted. Cost considerations and dispersion/chirp penalties must be weighted when deciding what transmitter source to use. Externally modulated lasers using $LiNbO_3$ Mach–Zender modulators are one solution. Transmitter sources like directly modulated distributed feedback lasers (DM-DFBs) or electroabsorption (EA) modulator integrated DFB lasers (EA-DFBs) may be attractive solutions for their low cost. Both of the above transmitter types present frequency chirp at the output modulated waveform, and this chirp will interact with the fiber dispersion and affect the transmission performance. The effect of the interaction of the laser chirp with the fiber dispersion may be deleterious for the fiber transmission over long fiber lengths but also may help to increase the transmission distance [10]–[12], as will be discussed in the next section.

Another unique characteristic of the metro networks is the presence of thousands of kilometers of already installed fiber that can contain both old and newer fiber installations. Performance over older fiber can be significantly affected by high values of polarization-mode dispersion (PMD). The increased number of optical components present in the metro area networks also introduces detrimental effects due to optical crosstalk, PDL, and filter concatenation. In fact, components can be the significant limitation rather than the transparent medium. Finally, fiber nonlinearities, which present significant limitations in long-haul and undersea systems, need to be addressed in metro as well. It becomes obvious from all the above that one of the main drawbacks of transparency is the accumulation of a number of optical layer impairments that make the above problem complex [13]. All the above effects, including cost, need to be studied and budgeted during the network engineering phase.

One of the contributions of our work is in deriving a successful computer simulation methodology that can effectively be used for the topology design and engineering of the network. Because of the complexity of the underlying problem, the choice of an adequate computer representation of optical signals and network components is essential. Several commercial simulation packages are currently available. They all provide an accurate and effective way of studying the performance of the transport layer for point-to-point optical systems using the well-known time/frequency simulation approach [14]. However, the computation time required for simulating large multiwavelength optical networks makes this approach time consuming and impractical in many cases. We have sought to develop a flexible tool capable of simulating a large number of network configurations. Our methodology is based on a three-step computer simulation approach: the first step involves performing a computationally efficient wavelength-domain simulation of the entire network [15] followed by conventional time/frequency-domain simulations on identified worst case paths. Finally, a budgeting approach is derived based on accurate impairment models and information obtained from the previous two simulation steps to estimate the Q-performance of the network on these worst case paths. This provides an efficient simulation tool that will exhaustively simulate optical paths for different topological designs to help the network designer understand the physical layer limitations of each topology and assist with network engineering.

The above models are described in Section II of this paper along with experimental model validation. Section III introduces several model metro network architectures. Interest in mesh optical networks is constantly growing, and while not yet deployed, mesh designs are becoming quite popular in concept for extending the ring-based networks that are designed after the traditional legacy SONET rings. Our current study focuses on two variations of a ring architecture but can be easily extended to include mesh or any other network design. Section IV illustrates that topology design and engineering of these transparent networks is feasible using the appropriate methodology aided by computer simulation and examines each one of the above performance impairments in greater detail. Network size and parameter tradeoffs are also presented for each metro design examined. Section V provides the conclusions for our work.

II. Simulation Methodology

Computer simulation can be effectively used for managing the complexity of engineering metro WDM optical networks, without sacrificing the need for topological flexibility. During the last few years, a number of simulation packages intended for the network optical layer have emerged. The operation of the majority of these tools is based on the well-known time- and frequency-domain simulation principles [14]. In order for a signal to be effectively represented in the computer, sampling of either its time-domain (waveform) or its frequency-domain (spectrum) representation has to be performed with a sampling rate that follows the Nyquist criterion [16]. Both frequency- and time-domain representations are equivalent, and transition from one to the other is performed by means of a Fourier transform. Unfortunately, simulation of WDM optical communication networks requires a large simulation bandwidth mainly because of the large aggregate bandwidth of the optical signals and the wide range of the ASE noise. Moreover, such networks contain a large number of optical paths over which these time-/frequency-domain simulations need to be performed. To reduce the sampling frequency, a low-pass (equivalent) representation of the narrow-band signals can be used [17], but the computational complexity remains large. To gain in simulation speed, it is essential that we increase the resolution bandwidth of the simulations. This will result in loss of accuracy and will eventually prohibit the simulation from switching between time and frequency domains since the Nyquist criterion will be violated and aliasing will occur. In many cases, simulation speed is a significant constraint and must be achieved with minimal sacrifice in accuracy.

The *wavelength-domain* representation that increases speed by increasing resolution bandwidth is presented in great detail in [15]. The approach essentially consists of undersampling the various spectra and ignoring the phase of the signals, which means ignoring their modulation and representing their spectra by simple impulses in the frequency domain. The main assumptions in doing so are that the frequency characteristics of typical optical components (i.e., MUX/DMUX, optical amplifiers) generally vary slowly within the individual signal bandwidths and can be effectively described in this domain in terms of the values of their transmittance transfer functions (gain, loss) and that ignoring the modulation of the carriers does not affect the behavior of the amplifiers. A result of the undersampling performed in wavelength-domain simulation is that switching between time and frequency domains is not possible. However, this is not needed since this approach is used to calculate the average signal powers and optical signal-to-noise ratio (OSNR) and not to evaluate the waveform evolution of channels through the optical components of the network. In addition, all types of linear crosstalk terms generated at each of the network components can be collected when wavelength-domain computer simulation of a network is performed, as shown in [18]. Since no modulation, phase, or polarization information for signals is propagated in the wavelength domain, the collected crosstalk terms are simply represented in terms of average powers and are stored separately as distinct narrow-band optical signals. The crosstalk-induced penalty in the network must be evaluated during another simulation step (second step), performed in the time domain. Moreover, nonlinear effects in the fiber and other optical components, as well as polarization effects, are not captured in the wavelength-domain simulations and are studied only on individual paths of the examined networks as part of the time-domain simulation step.

Our simulation methodology then is based on three consecutive steps:

1) wavelength-domain simulation of the entire network;
2) time-/frequency-domain simulations of identified paths;
3) budgeting analysis on the worst case path.

The first step consists of performing wavelength-domain simulation of the whole network to obtain a first-cut understanding of its performance. During this step, average signal powers, ASE noise, and linear crosstalk are obtained at every point in the network. More than one iteration of the simulation may be needed to calculate all possible crosstalk terms in topologies such as rings and for the spectrally resolved model of the erbium-doped fiber amplifier (EDFA) to produce accurate results [19]. During the second step of the simulation, the optical network is decomposed into worst case paths based on the OSNR and crosstalk information available from the wavelength-domain simulations and by identifying the major impairments present. We generally expect dispersion and fiber nonlinearities to be more pronounced on the longest paths in the network. Crosstalk, signal power divergence, ASE noise accumulation, PDL, and signal distortion due to optical filtering can be more detrimental in paths where the signal traverses a large number of optical components. Such paths exist in a typical metropolitan-area network and will be illustrated in more detail in the next section. For the identified possible worst case path(s), time-/frequency-domain simulations are performed using conventional split-step Fourier approach to determine channel performance in that path. Using the above simulation methodology allows us to perform complex and time-consuming time-/frequency-domain simulations only on specific worst case paths rather than on the entire network.

The performance of transmission systems is often characterized by the bit error rate (BER), which is required to be smaller than approximately 10^{-15} at the beginning of life for most installed systems. Experimental characterization of such systems is not easy since the direct measurement of BER takes considerable time at these low BER values. Another way of estimating the BER is to degrade the system performance by moving the receiver decision threshold value, as proposed in [20]. This technique has the additional advantage of giving an easy way of estimating the Q of the system, which can be more easily modeled than the BER. The parameter Q is defined as [21]

$$\mathrm{BER} = \frac{1}{2}\,\mathrm{erfc}\left(\frac{Q}{\sqrt{2}}\right) \simeq \frac{\exp^{\frac{-Q^2}{2}}}{Q\sqrt{2\pi}}. \tag{1}$$

The Q-penalty of a system is often expressed in dB. Since we are mostly concerned with the optical penalties introduced by different impairments, we will use the following definition for dBQ throughout this paper:

$$\mathrm{dBQ} = 10\log(Q_{\mathrm{linear}}). \tag{2}$$

The second part of the simulation methodology described above can be used to provide the penalties (in dBQ) due to fiber nonlinearities, polarization effects, and linear optical crosstalk that cannot be obtained using the wavelength-domain approach of step one. The time-/frequency-domain simulations that are constructed for the identified worst case path of the optical network provide a very accurate approach in dealing with the various detrimental effects in the optical path. However, they are time consuming and may need Monte Carlo statistics to deal with the randomness of the phase and polarizations of the channels. When trying to engineer the performance of an optical network, we need a tool that will be flexible and fast enough to run simulation repetitions for different network parameters and network sizes, and the above simulation approach by itself cannot be effectively used. A third simulation step is thus needed that uses information from the previous two steps to determine the Q parameter for the channels on the worst case path in a simple and time-efficient way. This is a budgeting approach where dBQ penalties for the various effects obtained either from the second step of the simulation methodology presented above or through impairment models are used. The Q performance of all the channels applied on the worst case path can then be calculated by keeping track of the signal and ASE noise powers starting from the optical transmitter, through the various components, and finally at the optical receiver taking into account channel power divergence, dispersion/chirp, ASE noise, receiver noise terms, and budgeting for all other impairments in the form of dBQ. It must be noted that this is different from a simplistic Q-budget since the margin allocated for each impairment is not a fixed amount but is calculated from a corresponding impairment model. The main limitation of the above overall approach is the tradeoff of accuracy with speed. During the implementation of the final step (i.e., budgeting analysis on the worst case path) in trying to do the network engineering, certain parameters may change. Ideally, then all three steps of the methodology would need to be repeated each time a parameter change occurs increasing the simulation time. In our work, we assumed that parameter changes provide a minimum change in the overall impairment budgeting of the network and thus avoided any iterations.

The rest of this section describes in more detail the different impairments along with the models used in our simulations as well as some model validation results.

A. Signal Power Divergence

The reach of a system is usually roughly optimized if the powers (or OSNRs) of the individual channels are uniform. However, signal power or OSNR imbalance can result from imperfections in the loss/gain functions of optical components such as MUXs/DMUXs, optical amplifiers and couplers, PDL, or dynamic reconfigurations of the network that add/drop channels at different power levels. Signal power divergence accumulates as the channels propagate through an optical path. The impact of this effect on the network performance can be very significant as the low power channels can be affected by receiver electrical noise and low OSNR, whereas the strongest ones can potentially reach the regime where nonlinear effects become important, as shown in [22]. The dynamic range requirements imposed on the optical receivers can limit performance. This issue has been studied in networks and systems before [23], [24], but it has not been quantified in metro networks where the number of possible traversed components is larger than in long-haul systems. The above effect is taken into account during the first step of our simulation procedure when signal and noise powers are propagated as part of the wavelength-domain simulation. The use of dynamic power equalizers provides an effective solution for the mitigation of the above effect, and its benefit in our particular metro network design will be demonstrated in Section IV.

B. Chromatic Dispersion/Chirp

Recently, cost-effective directly modulated lasers (DMLs) have attracted much attention for 2.5-Gbps operation at both 1300- and 1550-nm wavelength bands for applications in metropolitan-area systems and in networks [25], [26]. They present the advantages of small-size, low-cost, low driving voltage, and high available output power. However, their major drawback is that their chirp characteristics can significantly limit the maximum achievable transmission distance over conventional single-mode fibers [27]. Due to the high positive value of the linewidth enhancement factor (α) of the semiconductor material, the leading edge of the pulses is blue-shifted relative to the center of the pulse while the trailing edge is red shifted. At 2.5 Gbps, the 2-dB power penalty chirp/dispersion-limited distance (usually referred to as the laser rating) of commercially available 1550-nm DMLs is typically 1800 ps/nm. At 10 Gbps, this distance is much lower (usually less than 10 km due to high laser chirp). EA modulator integrated DFBs are another possible solution as 10-Gbps 1550-nm sources for metro network applications, as they can transmit signals somewhat beyond the dispersion limit when used in the negative chirp regime [12]. Commercially available EA-DFBs are specified for a dispersion tolerance of 1440–1600 ps/nm (about 80–90 km of single mode fiber) at 10 Gbps. However, their output power is rather small (5–10 dB lower than that of DMLs) presenting a different power budget requirement than the DMLs. From the above, it is clear that the interaction of laser chirp and fiber dispersion is very critical for the design and engineering of metro networks where transmitter technology and cost are the major issues. Many models exist in the literature that are able to describe all the characteristics of the modulated waveforms at the output of the transmitters, for example, [28]. For instance, the rate equation model can be used to simulate the behavior of DMLs [10], [11], while a phenomenological model can be used to predict the behavior of EA-DFBs [29]. However, in this study, a more simple approach has been used. The effects of the laser frequency chirp and fiber dispersion have been taken into account in a simple phenomenological model that is able to predict the dispersion/chirp-induced eye-closure penalty. The model uses parameters measured in the lab, and its accuracy has been tested against the experiments. In the case of chirp-free signals, the dispersion-induced penalty P (dB) is calculated using the expression

$$P\,(\text{dB}) = 10\log\left(\frac{1}{1-\gamma L^2}\right) \tag{3}$$

where γ is directly proportional to the level of intersymbol interference and L is the transmission link length. This kind of penalty dependence on the transmission link has been also calculated using transmission simulations [29], [30] and has been verified by experiments. As shown in [30], the level of intersymbol interference induced by the dispersion will be proportional to

$$\gamma \sim \frac{\lambda^4 D^2 B^4}{c^2}. \tag{4}$$

A fitting constant is then added to the expression for the γ-parameter in order for the dispersion-induced penalty to match with the results produced by the transmission simulations of [29] and [30] and with experimental data. In fact, a worst case approach is followed, where the model is matched with the most

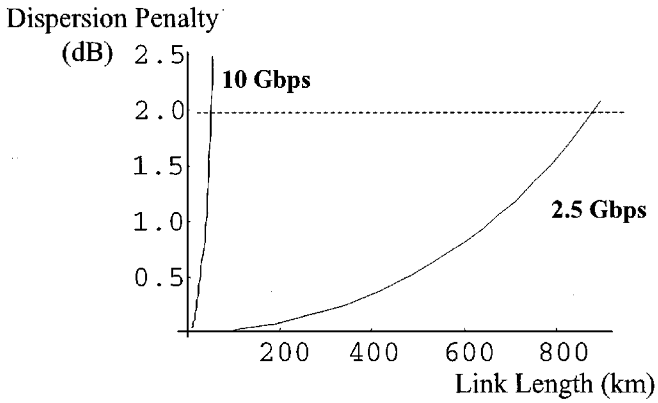

(a)

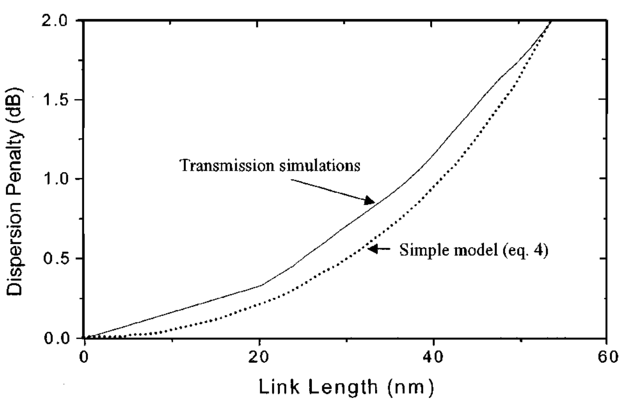

(b)

Fig. 1. (a) Theoretically calculated [based on (3) and (4)] dispersion-induced penalties for an ideal chirp-free signal at 2.5 and 10 Gb/s (the signal wavelength is assumed to experience 17 ps/nm-km dispersion). (b) Comparison of dispersion-induced penalty for a chirp-free 10-Gb/s signal versus distance (km) as calculated from (3) and (4) (dotted line), with transmission simulation results performed using a chirp-free ideal waveform with infinite extinction ratio (solid line) [28].

conservative available data. Fig. 1(a) shows the calculated dispersion-induced penalty for an ideal chirp-free signal at 2.5 and 10 Gb/s (the signal wavelength is assumed to experience 17 ps/nm-km dispersion). As calculated from (3), the 2-dB dispersion-induced penalty occurs at about 55 km for a 10-Gb/s signal and at about 900 km for a 2.5-Gb/s signal. Fig. 1(b) compares the dispersion-induced penalty for a chirp-free 10-Gb/s signal versus distance (km) as calculated from (3) and (4) (dotted line), with transmission simulation results performed using a chirp-free ideal waveform with infinite extinction ratio [29] (solid line). A close agreement is observed, verifying the validity of the model.

In the case of chirped signals, we use a phenomenological model based on the concepts presented in [31] and [32]. As is well known, signals produced by DMLs and EA-DFBs exhibit frequency chirp, which in the case of DMLs is always positive (blue-shifted leading edge of the pulse; red-shifted trailing edge) due to the positive value of the α-parameter of the semiconductor material. In the case of EA-DFBs, the chirp is tunable and may be positive or negative (red-shifted leading edge of the pulse; blue-shifted trailing edge). Positively chirped signals spread after transmission over positive dispersion fibers and cause intersymbol interference that deteriorates significantly the quality of the received signals. However, positively chirped signals are expected to perform very well over negative dispersion fibers since some pulse compression will take place. The opposite effects will occur in the case of negatively chirped signals. Since in metropolitan-area networks we have a coexistence of both positive (SMF-28[1], LEAF[2]) and negative (MetroCor[3] fiber, dispersion compensating modules) dispersion fibers, a simple, systems-oriented model that is able to predict the amounts of positive and negative chirp-induced penalties due to pulse spreading or compression, respectively, is of particular importance. Following a similar approach as that presented in [31], we assume that the pulse waveform is an ideal square and that the leading and trailing portions of the pulse are chirped. Fig. 2 illustrates our assumptions more clearly for the case of a positively chirped signal. The pulse exhibits a finite extinction ratio, and the power levels of the "1" and "0" bits are denoted as π_1 and π_0, respectively. The chirp (measured in nm) is assumed to have a peak value of $\Delta\lambda_c$, and the duration of each chirped portion of the signal is t_c (measured in nm). From the values of t_c and the average pulse power, the chirped signal power can be calculated. The chirped signal power will compress/spread the pulse proportionally to the term $D \times L \times \Delta\lambda_c$, where D is the fiber dispersion and L is the fiber length. If we assume that a signal with such characteristics is transmitted through an optical fiber, the following can happen: in the event that D is positive, the pulse will start broadening since the blue-shifted portion of the pulse will start advancing relative to the center portion of the pulse, while the red-shifted portion of the pulse will be delayed (Fig. 2). The broadening will be much faster than that which dispersion will induce to a chirp-free signal, because of the positive laser chirp (nonoptimum prechirped transmitter). If D is negative, the pulse narrows because of the counterinteraction of chirp and dispersion (optimum prechirped transmitter). The blue- and red-shifted portions of the pulse will move toward the center portion of the pulse until a point of maximum compression. From this point on, the pulse will start broadening again. In both cases, the amount of power that enters/exits the bit period (corresponding to the chirped signal power) has been assumed as increasing linearly with distance along the fiber until all chirped power has entered/left the bit interval [31]. Based upon this approach, it is evident that pulse narrowing results in an increase in the average level of the ones (represented as π_1 in Fig. 2) resulting in eye-opening and performance improvement, whereas pulse broadening will result in an increase in the average level of the zeroes (represented as π_0 in Fig. 2) resulting in eye-closure and performance deterioration. The above two models for chirp and dispersion are then added together, and a model for the combined effect is obtained. Fig.3 presents simulation results of the above combined model for the case of transmission of a 10-Gb/s signal produced by an EA-DFB over a fiber link with a dispersion of 17 ps/nm/km. Three curves are shown: one for a chirp-free signal, one for a signal with optimum prechirping

[1]SMF-28 is a trademark of Corning, Inc.

[2]LEAF is a registered trademark of Corning, Inc.

[3]MetroCor is a trademark of Corning, Inc.

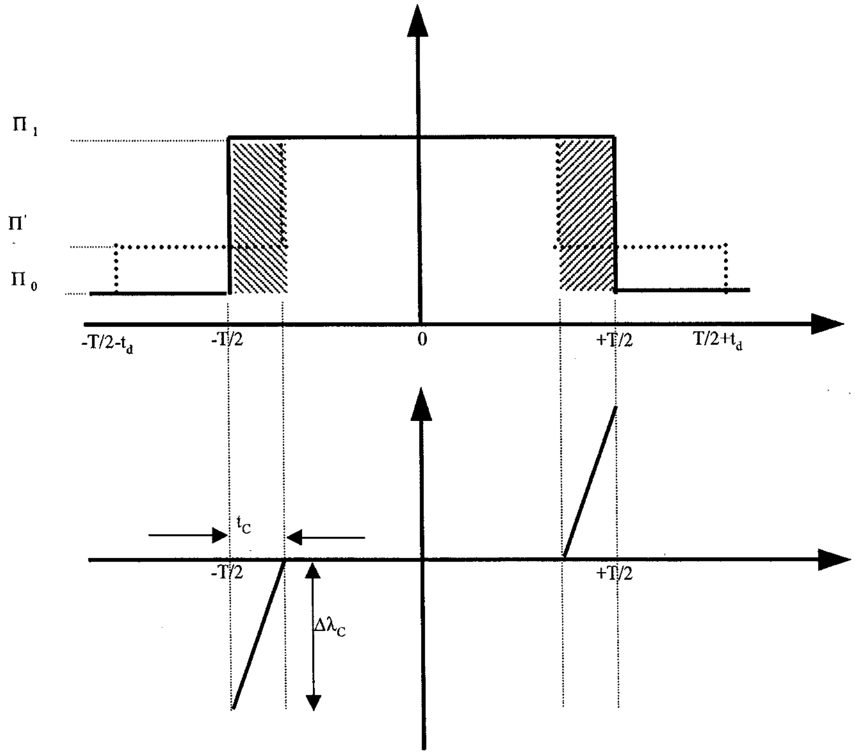

Fig. 2. Representation of a positively chirped signal as a means of explaining the phenomenological model for chirp presented in Section II-B. Knowledge of $\Delta\lambda_c, t_c$ and average pulse power is used to determine eye opening/closing in the system.

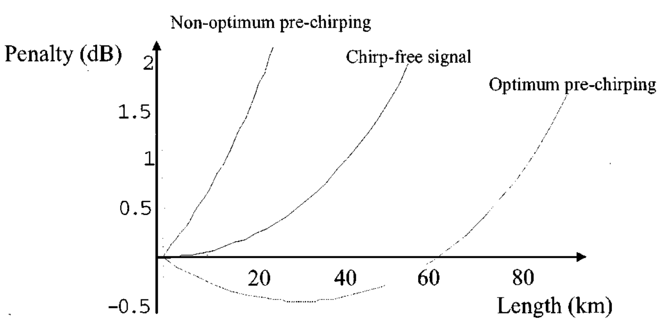

Fig. 3. Dispersion/chirp penalty (dB) versus optical path length (km) for a 10-Gbps signal using an EA-DFB transmitter and the phenomenological model of Section II-B. Chirp-free, optimum prechirping, and nonoptimum prechirping cases are demonstrated.

(i.e., positive dispersion fiber and negative chirp), and one for a signal with the same chirp characteristics $(\Delta\lambda_c, t_c)$ as in the previous curve but for nonoptimum prechirping (i.e., positive dispersion fiber and positive chirp). The model parameters had values that agreed with those measured in experiments for most of the EA-DFBs that we have tested ($\Delta\lambda_c = 0.02$ nm, $t_c = 35$ ps). For optimum prechirping, the 2-dB penalty occurs at a distance of approximately 95 km, in accordance with the Dispersion $\times$ Length rating of 1600 ps/nm for commercially available devices. The above model is general and can also be used for DML transmitters provided that the $\Delta\lambda_c$ and t_c parameters are obtained.

C. Polarization-Mode Dispersion (PMD)

PMD can be an important impairment in high-data-rate transmission systems and networks. It is defined as the statistical mean of the differential group delay (DGD) distribution. It has been shown that fiber, as well as other components made from fiber such as dispersion compensating modules, have Maxwellian DGD distributions [33]. When the above devices are put together, the mean value of DGD (i.e., PMD) adds in quadrature, producing the total PMD of the system. As an example of PMD budgeting, it has been shown that when 40% of the bit period is allocated for PMD, about 1 dB penalty can be budgeted for in the system with a 10^{-7} probability [34]. Based on the above budgeting scheme and assuming all the components in the network can have their PMDs added in quadrature, a total PMD value and penalty can be obtained and budgeted for during the second step of our network simulation procedure. The quadrature addition of PMDs for all the components has been shown to lead to conservative estimates of system PMDs at low probabilities [35]. However, for the purposes of this paper, it presents a satisfactory simple and relatively accurate model. It must be noted that the simplicity of the above impairment budgeting approach allows for an easy upgrade of the PMD model. As bit rates increase toward OC-768, a more detailed treatment of PMD may be necessary. Models such as that presented in [36] and [37] will provide a more accurate approach to PMD and can be easily incorporated in our methodology.

D. Linear Optical Crosstalk

Linear optical crosstalk has been a known major impairment in optical networks and has been extensively studied in the literature [38]–[44]. It is generated at optical components in the network due to the nonideal characteristics of MUXs/DMUXs and optical switches. Optical crosstalk can be distinguished into

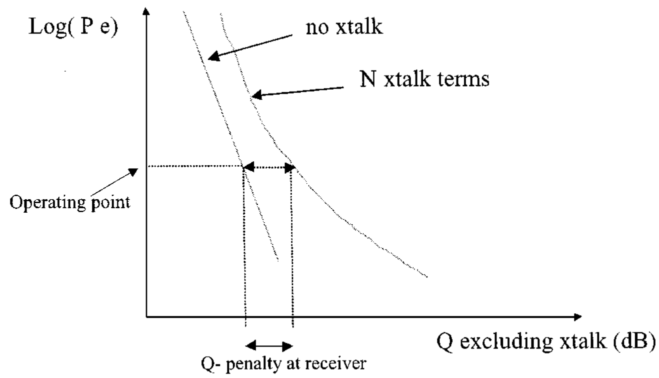

Fig. 4. Definition of crosstalk-induced Q penalty (dB) at the receiver of an optical path.

two major categories: common channel and adjacent channel. The former refers to optical crosstalk terms that have the same nominal wavelength as the signal, whereas the latter refers to cases where the terms have different nominal wavelengths. The common-channel crosstalk terms can originate from the same laser, in which case we refer to them as multipath, or from different lasers at the same nominal frequency. Common channel crosstalk terms are thus the most detrimental to the signal performance since they cannot effectively be filtered from the signal. When studying the performance of a metropolitan optical network where the signal can traverse through a large number of optical components, the number and relative strength of the generated crosstalk terms need to be obtained. The exact penalty that the crosstalk imposes on a channel depends on the modulation, frequency, phase, and polarization of the interfering electric fields. For our simulation work, a realistic assumption is that all crosstalk terms affecting a channel have traveled such diverse paths in reaching the receiver that their phase and polarizations are adequately random compared to the signal (uncorellated). We can thus use the wavelength-domain computer simulation approach to collect all the possible crosstalk terms accumulated over the whole network at a specific receiver and then use a theoretical model to determine the crosstalk-induced Q-penalty during the second part of the simulation. Crosstalk-induced Q-penalty is defined as the difference in Q (dB) at the optical receiver that is observed at a given error probability P_e for the case of no crosstalk in the system and the one that contains the effects of crosstalk in it. This definition is more clearly illustrated in Fig. 4. To achieve the above, the error probability of the point-to-point identified worst case path at the direct-detection receiver is accurately evaluated. The error probability calculation takes into account the presence of N copolarized interferers, ASE noise, receiver shot and thermal noise, and the non-Gaussian photocurrent statistics. For the evaluation of the error probability, we derive analytical expressions of the probability density function and the cumulative distribution function of the photocurrent at the output of the direct-detection receiver based on the formalism in [42] and [45]. The analytical expressions involve infinite series of Hermite polynomials and moments of the crosstalk-induced interferometric noise [45]. The aforementioned model for the photocurrent statistics has been generalized in [44] to include crosstalk–crosstalk and noise–crosstalk beatings, as well as the direct detection of the crosstalk and the ASE noise, which are neglected in [42], [45]. The model is also experimentally validated [44].

E. Polarization-Dependent Loss (PDL)

Lightwave systems and networks with a large number of optical components (such as undersea systems or metro networks) are vulnerable to performance degradations due to PDL. PDL may be caused by optical components such as directional couplers, isolators, filters, and band-splitters and is due to the variation of the insertion loss over the different polarization states of the optical device [46]. As a result, the total PDL along a particular optical path will depend on the initial signal polarization orientation and on the relative orientation of the polarization axes of each component in its path. Due to PMD, the principal states of polarization are randomly varied in a wavelength-dependent way, and as a result, the interaction of PMD with PDL introduces among other effects a wavelength-dependent variation of the loss/gain that each signal will experience in the path. This is most commonly known as PDL-induced ripple. Due to the statistical nature of polarization, this ripple effect can only be studied in a probabilistic way. We use a numerical Monte Carlo simulation model as described in [47] to derive the statistics of total PDL in a system along with the PDL-induced ripple effect. In this model, each component is represented as a birefringent element with random orientations of its principal axes. All signals propagate through these elements starting with some random orientation of their polarization axes. The PDL-induced ripple statistics are calculated at the receiver based on Monte Carlo simulation runs over a large set of axes' orientations. This model is used during the second part of the simulation methodology, focusing only on the intended worst case path in the metro network. A PDL-induced ripple is deduced from the simulations and used for engineering the network design, as will be explained in Section IV of the article.

F. Distortion-Induced Penalty Due to Filter Concatenation

A serious signal impairment that is unique to transparent optical networks is distortion-induced eye closure, an effect that can be produced by signal passage through multiple WDM filters between the source and receiver. This effect is essentially relatively small in a point-to-point optical system since a given signal passes through at most two filters: a MUX and a DMUX. However, in a transparent optical network, a signal may be demultiplexed and remultiplexed at many network elements throughout its path before it is finally received. Thus the signal experiences the concatenation of the entire set of filters in its path. The effective spectral transfer function of the filter set is the multiplication of each of the individual filters' transfer function, and can therefore be much narrower in spectral width than that of a single filter. The impact of spectral narrowing of the transfer function is exacerbated by any filter/laser center frequency misalignments. If the laser is offset from the center of the passband of the effective filter transfer function, then part of the signal spectrum can be attenuated relative to the rest of the spectrum as the signal gets too close to the edges of the filter transfer function. This in turn can lead to a time-domain distortion and a distortion-induced eye closure penalty that is related to Q penalty. The phase characteristics of each filter also contribute to the above distortion-induced penalty since they introduce dispersion whose absolute value and slope increases as the number of optical filters in the cascade increases. In [48], a comprehensive theoretical model for the study of the concatenation of optical multiplexers/demultiplexers in transparent optical networks is presented along with a detailed list of prior works on the subject such as [49]. The work in [48] takes into account intersymbol interference, ASE noise accumulation and filtering, arbitrary optical multiplexer/demultiplexer and electronic low-pass filter transfer functions, and non-Gaussian photocurrent statistics at the output of the direct detection receiver. To our knowledge, it presents the most general and accurate study on the subject. However, for the purpose of engineering the performance of a metro optical network, a simpler simulation approach is required. We adapt the approach presented in [50]–[52], where the propagation tool used for the second step of our simulation methodology is used to produce noiseless simulations of the signal propagation through the optical filters. The eye pattern at the output of the direct detection receiver is then obtained and the eye opening is calculated as a measure of the system performance. Consequently, the distortion-induced (DI) penalty is defined as

$$\mathrm{DI~(dB)} = 10\log\left(\frac{\text{eye opening } (N=0, f_c=0)}{\text{Avg power } (N=0, f_c=0)}\right) - 10\log\left(\frac{\text{eye opening } (N=m, f_c=x)}{\text{Avg power } (N=m, f_c=x)}\right) \quad (5)$$

where the eye opening after m filters assuming a laser misalignment of f_c is normalized with respect to the average received optical power. This is done in order to distinguish the distortion-induced penalty from excess loss that is caused by filter concatenation, which unlike distortion-induced penalty can be compensated using amplification [50].

Experimental results as well as the above transmission simulation model have shown that for 2.5-Gbps (OC-48) bit rate, adiabatic chirp-dominated DML lasers appear to have the worst filter concatenation performance for positive frequency laser/filter detunings [53]. For this case, filter phase is not taken into account since its effect at 2.5-Gbps bit rates is negligible for the number of filters considered. Therefore, we developed a Q-budgeting procedure for filter narrowing based on adiabatic chirp-dominated DMLs [53]. Our model was based on the assumption that the zero and one bits have different carrier frequencies. Therefore, the power of the ones and zeros will experience different attenuation when passing through the same filter function. According to the model, when the signal is detuned toward higher wavelengths relative to the center wavelength of the overall filter transfer function, then the spectral peak that corresponds to the zeros is attenuated more than that corresponding to the ones and the extinction ratio of the received signal improves. Alternatively, the extinction ratio (and the signal quality) degrades when the signal is detuned toward shorter wavelengths since the spectral peak corresponding to the ones is attenuated more than that of the zeros. Fig.5 compares experimental results (single points) with the theoretical Q-factor calculations (solid line) using experimentally obtained laser parameters, as described in [54]. The close agreement of experiment and simulation verifies the validity of the model.

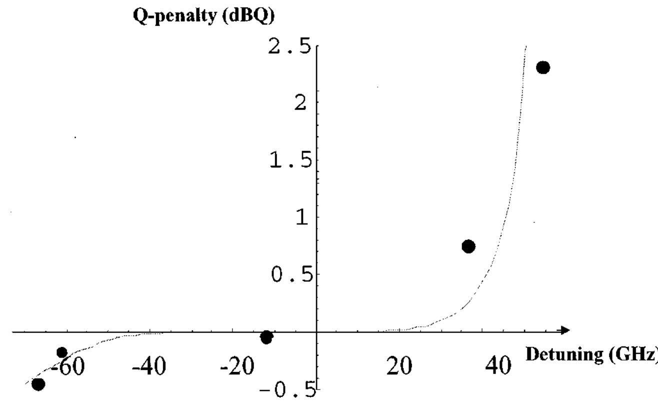

Fig. 5. Distortion-induced Q-penalty (dB) versus laser detuning for a 2.5-Gbps signal using adiabatic-chirp dominated DML transmitter. Experiment (single points) agrees well with theoretical model (solid line).

G. Fiber Nonlinear Effects

Fiber nonlinearities such as self-phase modulation, cross-phase modulation, and four-wave mixing are always a concern when designing a high-data-rate optical system or network [21]. In [22], it was shown that nonlinearities can become significant in the metro environment even for relatively low channel powers. For the purposes of this work, we used a link simulation tool to estimate the dBQ penalty for the fiber nonlinearities in the identified worst case paths of the examined metro network topologies. As discussed in Section IV, it is possible to design the network so that the total impact of fiber nonlinearities is small.

III. DWDM Metro Network Architectures

Fig. 6(a) and (b) presents the architectures for our metro network simulation case studies: single rings and transparently interconnected rings. Ring networks are used because of their inherent reliability. For both network designs, two-fiber rings with unidirectional traffic are assumed. One fiber is used for service traffic and the other for protection (1+1 protection scheme). The network of Fig. 6(a) models six distribution (or access) rings interconnected with an interoffice feeder (IOF) ring. Each access ring, depending on the demand, can interconnect N users (access nodes) that can, e.g., be small businesses, campus networks, or Internet service providers among others and can have a typical circumference of about 15–25 km. An important characteristic of these access rings is that they are passive, meaning that they have no amplifiers or optical switches, so that the design is kept simple, low in maintenance, and thus cost effective. Access rings are interconnected with the IOF ring using HUB nodes, which provide the cross-connect capabilities. However, it is possible that individual customers can also directly connect to the network through the HUBs. Traffic aggregation occurs at either the access or the HUB node sites and can involve a wide range of service types such as Internet protocol, asynchronous transfer mode, or frame relay over SONET/SDH and Ethernet.

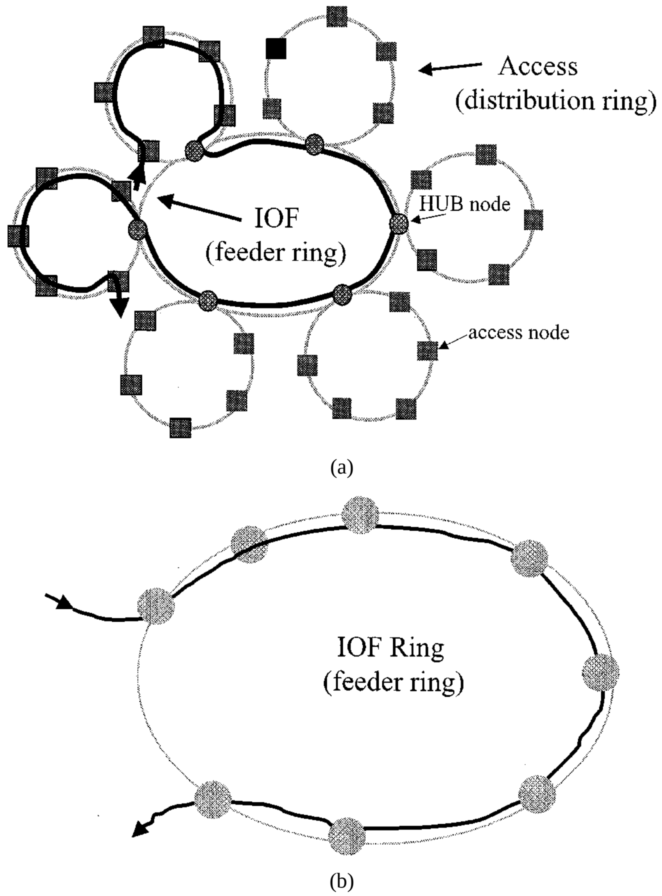

Fig. 6. Modeled metro network architectures: (a) interconnected ring topology and (b) single ring topology.

For the architecture of Fig. 6(a), it is assumed that client services are assigned the entire optical wavelength even if the demand does not reach OC-192 or OC-48 and that a mixture of access-to-access or access-to-HUB connections exist. At this time, however, much of the traffic in these networks is hubbed (i.e., access-to-HUB only) [55]. HUB nodes are used as the aggregation and in some cases the egress points to the long-haul backbone networks. As a result, in Fig. 6(b) this scenario is presented in the form of a single IOF ring with N HUB nodes interconnected with fiber spans of several kilometers.

Thirty-two channels are considered in the network, and these are partitioned into two major bands (C- and L-bands). Each band is further partitioned into two-to-six other subbands with individual wavelengths spaced 200 GHz apart and a guard spacing between bands. This guard spacing is imposed by the limitations of the optical band-filtering technologies. The idea of banding is very important since it allows hierarchical multiplexing/demultiplexing at each access or HUB node [3]. In many cases, it is not necessary for every wavelength to be demultiplexed at every HUB node if it carries no traffic for that specific node, and so optical node bypassing is a very cost-effective solution that also results in reduced insertion loss on the signal through path compared to single channel add/drops. Allowing for band-level demultiplexing provides each node with a range of wavelengths over which it can transmit/receive and thus ensures high connectivity within the network design. Fig. 7 presents a functional diagram of the physical layer of a HUB node assuming two distinct possible designs: (a) the case where the fiber is demuxed/muxed down to the individual wavelength level and (b) the case where demuxing/muxing happens down to the band level. In both cases, two options exist in terms of switching: (a) an optical wavelength (or) waveband switch provides the required reconfigurability or (b) a static design simply *hardwires* a connection from an incoming fiber to an outgoing one. For the purposes of this paper, full wavelength demultiplexing in the C- and L-bands along with a reconfigurable switch fabric is assumed for each HUB node. Several overlays are possible for the IOF ring for both networks shown in Figs. 6(a) and (b), in which case the size of the switch fabric inside the HUB node varies. For our case study, no ring overlays are assumed and a typical insertion loss for the switch fabric is used. The physical layer model implementation diagram of each HUB node used in this analysis is diagrammed in Fig. 8. It consists of two input and two output fibers corresponding to the access and IOF rings. The same HUB node design is repeated for the protection path and is physically distinct from the working path to avoid single-point of failure situations. The C- and L-bands are demultiplexed at the input using a band DMUX (only the C-band part of the design is shown), and a dispersion compensating module (i.e., a negative dispersion length of fiber) is used to compensate for the dispersion on the IOF ring. Dispersion compensating modules are not used on the access ring side of the HUBs due to the insertion loss of these modules. Optical amplification is provided at the input and output of the HUB nodes, and the C- and L-bands are demultiplexed down to the individual channel level. An optical switch provides the necessary network reconfigurability by adding/dropping or switching each channel, and power equalization modules after the multiplexers will provide the necessary dynamic power equalization, as will be discussed in the next section. The details of amplifier design, MUX/DMUX, and optical switching are beyond the scope of network engineering and topology design on which this paper focuses. As a result, these elements are represented using *black box* models with certain noise figure, crosstalk, and filter characteristics (Table I). Access nodes are assumed to be implemented using a serial design that provides for the add/drop of the appropriate band on the first level (band mux/dmux pair) and then selects the appropriate channel on the second level (channel mux/dmux pair). The goal of this work is to derive a network design that can be upgradable to higher bit rates without the need for costly equipment modifications, so we initially investigate performance at OC-48 with an upgrade path to OC-192. The main simulation parameters used in our study are shown in Table I.

IV. Topological Design and Network Engineering

In designing the metro networks presented in Section III and in trying to engineer their performance, we use the three-step simulation process outlined in Section 2. This process, which is based on monitoring the performance of the highest and lowest power channels (out of all the available channels) on the worst case path of the network, is a rather conservative approach but provides us with the necessary safety margin for our work. Fig. 6(a) and (b) illustrates the worst case paths for our network

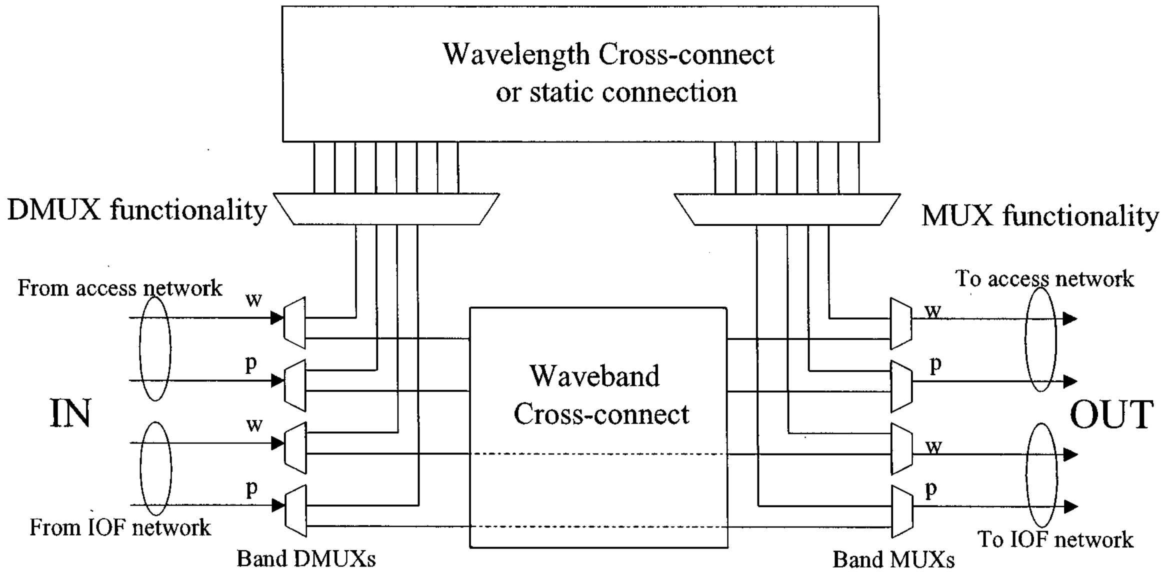

Fig. 7. Functional diagram of the physical layer of a HUB node.

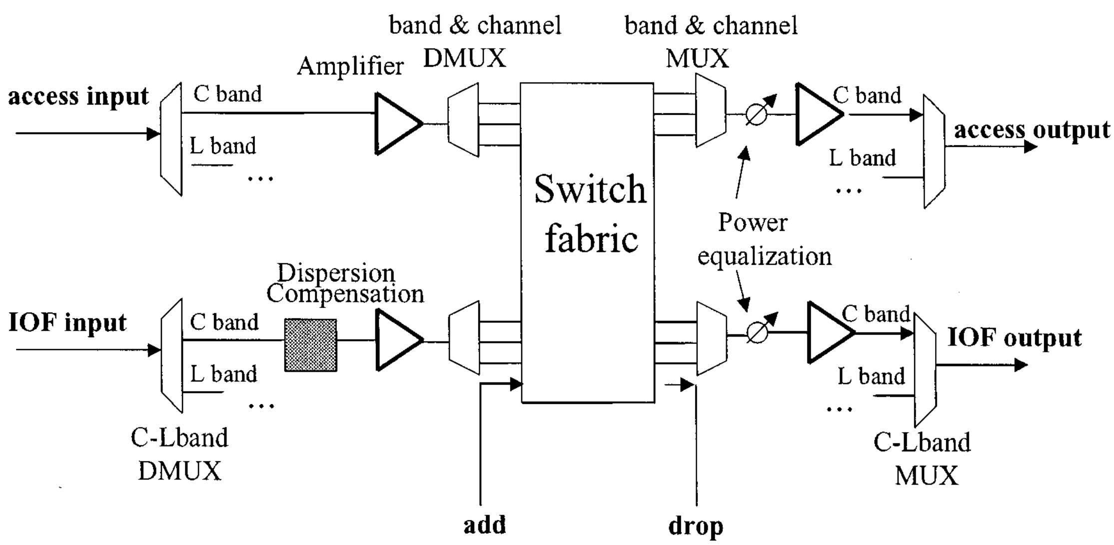

Fig. 8. Physical layer model implementation diagram of each HUB node used in our simulation analysis.

case studies; these paths happen to be the longest as well as the ones that pass through the most optical components for these particular designs. In the case of the six interconnected ring design [Fig. 6(a)], the optical signal is added on the first node of an access ring, traverses the whole access and IOF rings, and is dropped at the most distant node of the last access ring. In the case of the single IOF ring design [Fig. 6(b)], the optical signal is added and dropped at two adjacent HUBs, thus traversing the longest possible path on the ring. As a result, the protection traffic paths for the above two working traffic paths will span the minimum distances possible. It is also a general assumption in our network designs that each connection from node A to node B is accompanied by a return path connection from node B to node A using a transmitter at the same nominal frequency. This will become important during the study of crosstalk contributions presented below.

Besides engineering the performance of the above networks, this work deals with the topology design question of how big a transparent network can we support based on the initial ring architectures. We first focus on the network of Fig. 6(a), which is a more general version of the network of Fig. 6(b), and assume OC-192 (10 Gbps) bit rate, which needs to be supported as a direct upgrade path for the OC-48 (2.5 Gbps) case. During this study, three important network parameters have been identified:

1) power at the receiver (depends on channel launched power and loss on the final access ring);
2) OSNR at the receiver;
3) total uncompensated fiber length on the worst case path.

The interplay of the above three parameters can affect the size of the network that can be supported. For example, it becomes apparent that since the access rings of the examined design are unamplified, the total loss that can be supported on each one of these rings will be directly proportional to the channel power launched at their input. This is because at OC-48, the performance of the weakest channels will be limited by OSNR and receiver electrical noise if power drops below a certain

TABLE I
PARAMETERS USED IN THE SIMULATION STUDY

	2.5 Gbps	10 Gbps
Optical Bandwidth (Bo) (GHz)	62.5	62.5
Electrical Bandwidth at Receiver (GHz)	1.625	6.5
Noise Equivalent Circuit at Receiver (NEC) pA/sqrt(Hz)	2.745	14.45
Receiver sensitivity (dBm at 10^{-10})	-30	-29
Receiver Type	APD	Pre-amplifiedPIN
RIN of transmitter (dB/Hz)	-145.23	-145.23
Extinction Ratio (ε) (dB)	8	10
Responsivity (A/W)	1	1
Fiber loss (dB/km)	0.3	0.3
Peak-to-Peak chirp (nm)	0.085	0.02
Chirp Duration (ps)	85	35
HUB "black box" Noise Figure from the access ring side (dB)	7.8	7.8
HUB "black box" Noise Figure from the IOF ring side (dB)	17.8	17.8
HUB "black box" Noise Figure from the add side (dB)	11.0	11.0
Access node pass-through Insertion loss (dB)	2.3-3.0	2.3-3.0
Access node drop insertion loss (dB)	5.4	5.4
Access node add insertion loss	3.9	3.9
Transmitter type	DML	EA

level. The total loss that can be supported on each access ring will also depend on the sensitivity of the receiver, which, however, is assumed to have a fixed value. This maximum insertion loss that is supported can be allocated to individual node insertion loss (i.e., add/drop loss) and to fiber loss. Node insertion loss is proportional to the number of wavelengths or bands that are added/dropped at each node, however. Access to a large number of wavelengths translates to high node connectivity, which in turn reduces connection blocking in the network. It is desirable to be able to support big enough rings to connect a large number of geographically diverse customers, in which case fiber dispersion becomes a critical limiting attribute. In the model network used here, dispersion is not compensated for the fiber on the access rings, constraining total reach. Dispersion compensation happens only within the IOF rings using negative-dispersion fiber spans (i.e., dispersion compensating modules) at the input of each HUB node. As a result, Q-penalty due to chirp/dispersion will affect the performance of signals within the access rings much more compared to the IOF ring. On the IOF ring, we use modules that each compensate approximately 340 ps/nm of dispersion. However, these modules do not compensate for the slope of dispersion within the channel plan. As a result, depending on the length of each IOF fiber span, some channels are overcompensated whereas others are undercompensated, causing Q-performance variations. Channel launched power is limited by the ability of the amplifiers in the HUB to provide enough output power at a reasonable cost and by fiber nonlinearities on the access rings. The requirement for higher channel power will drive the cost of each amplifier higher since it will require more pumps. Channel launched power is also limited to the region where fiber nonlinearities are not dominant. Our studies have shown that +4 dBm launched power per channel presents a reasonable compromise value. The Q-penalty due to nonlinearities obtained for our 32-channel system, calculated using time-domain simulations, is approximately 0.1 dB, which is very small and is included in the impairment budget for the rest of this paper. The OSNR performance mainly depends on the number of amplifiers that the signal has traversed and limits the size of the IOF ring (i.e., the number of traversed HUBs and span length). Another effect that can potentially degrade network performance significantly is the nonlinear effect of the dispersion compensating fiber. In certain cases, relatively high total power into this fiber combined with narrow channel spacing and the fiber's small effecting area can create significant nonlinear effects. In our network, however, none of the above factors was present and thus no significant nonlinearities were observed.

To evaluate the tradeoffs among OSNR, dispersion, and received power, we performed a parameter variability study where we calculated Q performance for all the channels transmitted over the network for a reasonable set of combinations of the above parameters. We used simple budgeting rules and required that the Q-performance of the worst case channel be better than 8.5 dB, which corresponds to a BER of 10^{-12} at the end-of-life of the system. Fig. 9 presents contours of uncompensated single mode fiber length as a function of received signal power and OSNR for the case where +4 dBm per channel is launched into the final access ring as well as in each IOF span for the worst case path of Fig. 6(a). To begin the network design, we choose a typical set of parameters: in this example, an OSNR of 29 dB

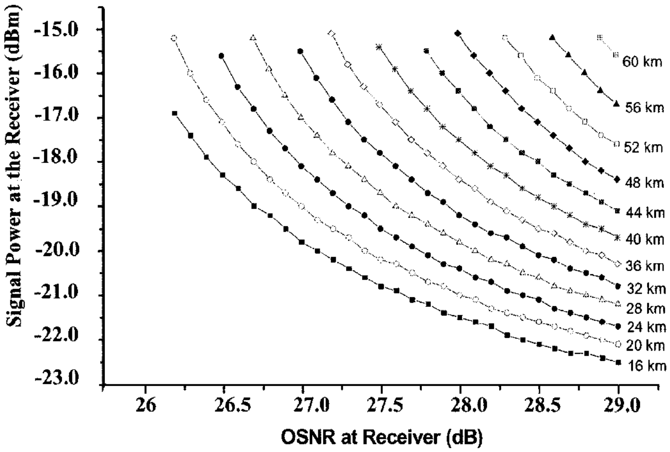

Fig. 9. Contours of uncompensated single mode fiber length as a function of received signal power and OSNR. This presents a network variability study for the worst case path of Fig. 6(a).

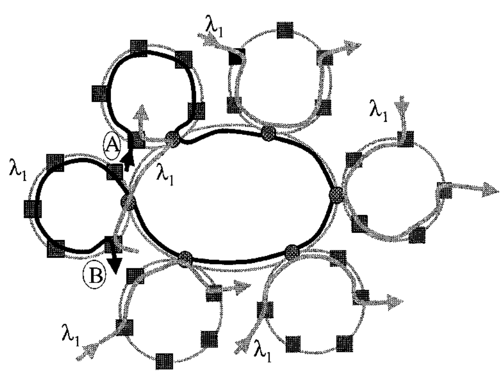

Fig. 10. Simulated worst case path for crosstalk accumulation. Signal path (dark line) will be collecting common-channel crosstalk terms generated by signals at same nominal wavelength (gray lines).

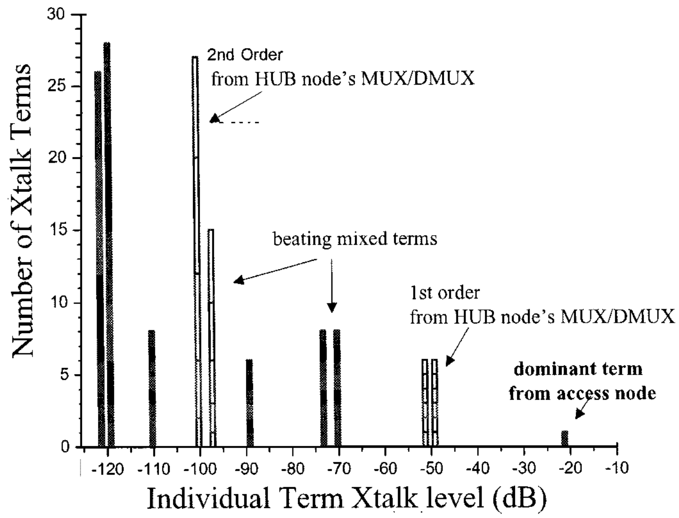

Fig. 11. Histogram of all crosstalk terms accumulated at receiver B of worst case path of Fig. 10. Dominant term is at -21 dB below the signal level and is caused by filtering imperfections at add/drop node A of Fig. 10.

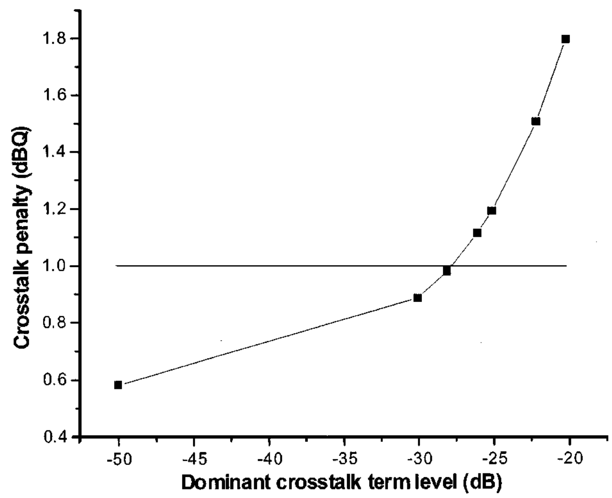

Fig. 12. Crosstalk-induced penalty (dB) versus dominant crosstalk term power level for the simulated worst case path of Fig. 6(a).

along with 32 km of uncompensated fiber, which will correspond to 16 km of uncompensated fiber per access ring on the worst case path. The above combination yields a required signal power at the receiver of about -21 dBm, which, assuming no in-line amplification for the access rings, will correspond to 25 dB of supported total insertion loss per access ring (Fig. 9). Based on the topology of Fig. 6(a) and these parameters, an initial design of the network can be obtained as follows: assuming an initial pass-through access node insertion loss of 2.3 dB (i.e., one band add/drops per node) and the add/drop insertion loss values shown in Table I, we can then design each access ring to consist of 16 km of single mode fiber and seven access nodes. Initially, we investigate network performance assuming six HUB nodes (i.e., six interconnected access rings). The size of the IOF ring can be further expanded during the study of the topology of Fig. 6(b) later in this section.

Wavelength-domain simulation is first performed to calculate OSNR, channel power level, and crosstalk information for the network. Wavelengths are routed in such a way that worst case crosstalk is produced. In particular, we focus on a given wavelength λ_1, which travels the worst case path shown in Fig. 10, and assume that λ_1 is being reused at each access ring in the network as well as for the return path from node B to node A. The received signal at node B will contain a large number of common channel crosstalk terms that have accumulated due to imperfections on filtering and switching at the different HUB nodes as well as at access node A. Fig.11 presents a power-level histogram of all the common channel crosstalk terms present at node B, which are obtained from wavelength-domain simulation. The strongest crosstalk contribution shown in Fig. 11 is generated at access node A and is due to the return path signal (light gray color on Fig. 10). Part of this dropped signal will leak and combine with the added signal (same nominal frequency) due to imperfections in the isolation of the band mux/dmux pair used at each access node (described in Section III). The power level of the added signal as well as the filter isolation performance will be the determining factors for this effect. In our example, this crosstalk term is -21 dB below the signal level and dominates over all other terms, which are on the order of -40 dB. The power levels of the 30 most dominant crosstalk terms are then used in time-domain simulation on the identified worst case path, and the Q-penalty (as defined in Fig. 4) is calculated using the crosstalk model described in Section II-D.

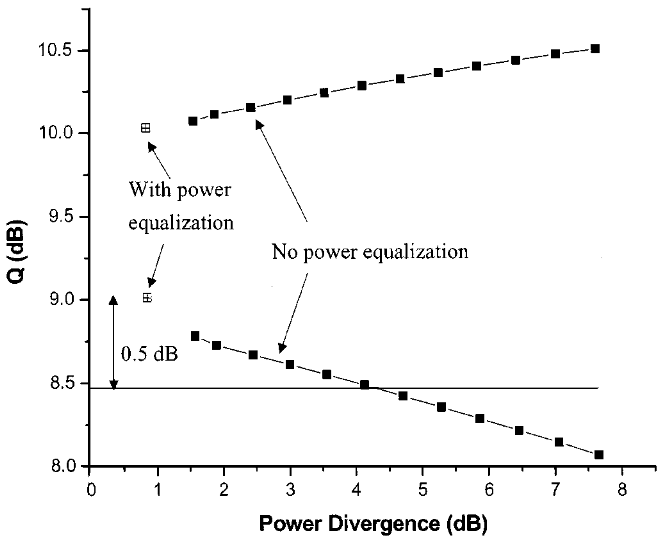

Fig. 13. Q (dB) channel performance for the strongest and weakest channel versus signal power divergence in the worst case path of Fig. 6(a). Results are shown for both the case where no power equalization exists in the network and the case where power equalizers are used at each HUB node.

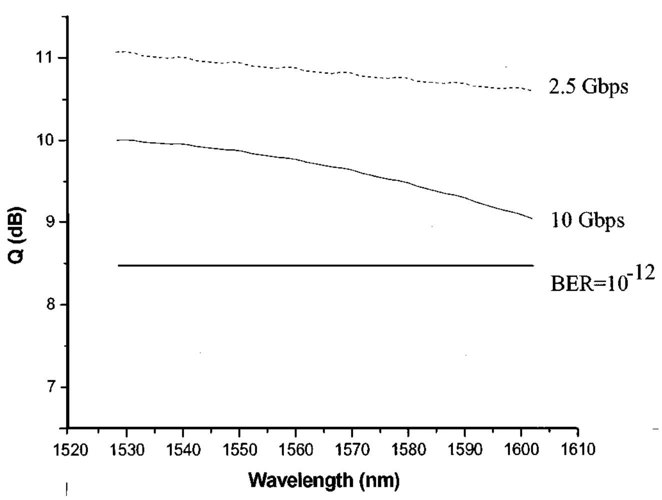

Fig. 14. Q (dB) channel performance for the worst case path of Fig. 6(a) versus wavelength. Results are presented for both the OC-48 case (dotted line) and the OC-192 upgrade (solid line).

Fig. 12 shows the obtained Q crosstalk penalty versus the different levels of the dominant crosstalk term. It becomes obvious that tighter crosstalk level should be achieved at each access node in order to maintain a 1-dB Q penalty as a target crosstalk budget in our design. This crosstalk performance can be achieved by tighter crosstalk filter specifications on each band mux/dmux or by additional filtering at each access node with the side-effect of increasing the pass-through insertion loss of each one of these nodes to about 3 dB (up from 2.3 dB used before). If the latter solution is chosen, only five access nodes along with 19 km of fiber can now be supported. Each node can add and drop one band (in this case, a four-channel band is used, but this is just a model used to demonstrate the power of the analysis) and thus each access ring can potentially support up to 20 wavelengths out of the total of 32, which provides adequate network connectivity.

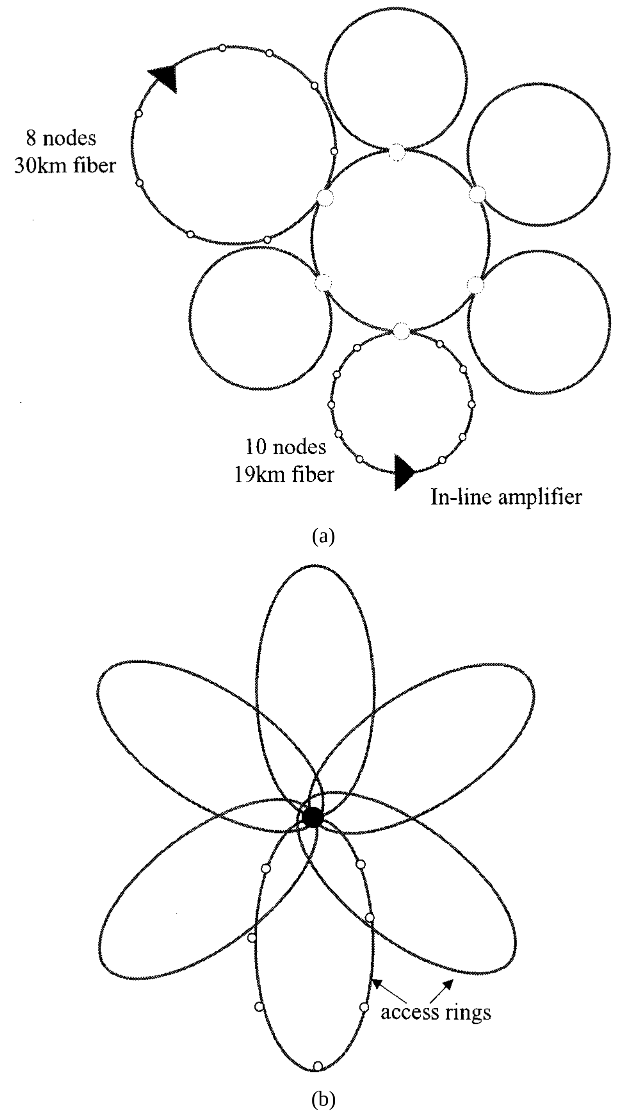

Fig. 15. Derived network size possibilities for (a) the interconnected ring design of Fig. 6(a) using in-line amplification in each access ring and (b) a modified network design where the IOF ring has been eliminated and access rings have been interconnected using a single cross-connect.

Based on this new design and assuming OC-192 connections using EA-modulated transmitters, time-domain simulation is performed on the worst case path to determine dBQ penalties for impairments such as distortion due to filter concatenation, fiber nonlinearities, and crosstalk. Penalties due to crosstalk and nonlinearities were very similar to those described for the initial seven access node network design. For filter concatenation, it was shown that a 1-dBQ distortion-induced penalty is an achievable budget value for DMLs at 2.5 Gbps, whereas EA-modulated and externally modulated transmitters at OC-192 perform better (0.5 dBQ distortion-induced penalty) [53]. Calculations based on the model for PMD described in Section II-C have estimated the PMD-induced dBQ penalty at 0.1 dB.

The final step of the simulation methodology consists of simple budgeting calculations based on the Q-penalties obtained above and focusing on the best and worst performing channels on the identified path. Fig.13 shows the Q-perfor-

TABLE II
DERIVED NETWORK SIZES FOR DIFFERENT CONFIGURATIONS OF THE SINGLE-RING NETWORK OF FIG. 6(b) AT BOTH OC-48 AND OC-192 BIT RATES

Bit rate	OC-48		OC-192	
Span lengths (km)	**# of HUBs**	**Ring size (km)**	**# of HUBs**	**Ring size (km)**
17	20	340	7	119
20	20	400	12	240
25	12	300	7	175
34	6	204	4	136

mance of the above two channels as the power divergence among them is allowed to increase, assuming no power equalization in the network. As the strongest and the weakest channels propagate through the optical components, their optical powers diverge and their performance in terms of Q-factor differs dramatically. The result clearly demonstrates that without the use of dynamic power equalization in the network, the weakest channels are not able to achieve acceptable performance even for a small total power divergence in the network of about 4.5 dB. With the equalizers present, all channels achieve performance better than the target $(Q \geq 8.47)$, and in addition a 0.5-dBQ performance margin is obtained. This can be used to relax the component specifications in the network for impairments such as crosstalk, filter bandwidth, and others. We therefore simulate a network that includes power equalizers at each HUB of the IOF ring (see HUB in Fig. 8). The effective noise figures at the nodes have been increased to account for the effect of power equalization.

Monte Carlo simulations on the effect of PDL have shown that with a probability of 99%, a 0.5-dB PDL-induced ripple will accumulate between each HUB of the network of Fig. 6(a). The power equalizers are then designed to handle the above ripple effect in addition to the component ripple that accumulates between HUBs.

Fig. 14 shows the final Q-parameter versus channel obtained using the described budgeting methodology on the final design of the interconnected metro ring composed of six interconnected access rings, each having five add/drops (with four-channel bands as an example), a total 38 km of uncompensated traveled fiber (19 km in each access ring), and 85 km of compensated traveled fiber on the IOF ring. Both OC-48 and OC-192 cases are engineered for all the channels on the worst case path taking into account the most important impairments, including an additional 1-dBQ margin for component aging in the network. For the OC-192 case, EA-modulated transmitters with a 1600-nm/ps commercial laser rating are used, whereas for the OC-48 case, adiabatic chirp-dominated DMLs with experimentally measured parameters are used (commercial ratings of 1800 ps/nm). The L-band channels perform worse than the C-band channels due to the increased fiber dispersion in this region of single mode fiber.

The above design and engineering procedure is very general and can be repeated for other network topologies. Fig. 15(a) illustrates the case where expanded network size is obtained by using in-line amplifiers in each of the access rings of the network of Fig. 6(a). Fig. 9 can still be used to obtain useful parameter tradeoffs assuming that the amplifier gain is included in the calculations of the total supported insertion loss and OSNR. Access rings in this case can be up to 30 km in total length supporting eight nodes or 19 km supporting ten nodes. Fig. 15(b) illustrates a different design in which the IOF ring has been eliminated and all access rings are now interconnected using a single cross-connect. This application can serve a densely populated metro area that is not geographically large. Simulations show that unamplified access rings with 19 km of total fiber can now support seven add/drop nodes. The single-ring network topology presented in Fig. 6(b) can also be analyzed based on the above methodology. Table II presents the results of such analysis assuming different fiber span lengths and bit rates exploring the maximum possible network size that can be supported. For all these cases, dispersion compensating modules that compensate for approximately 20 km of single mode fiber are used at each HUB node. At OC-48 and assuming 20-km fiber span lengths between the HUBs, we can achieve the largest possible ring (400 km in diameter) using either adiabatic or transient chirp-dominated DMLs with 1800-ps/nm commercial laser ratings. As the span lengths get shorter or longer, dispersion overcompensation on the C-band channels or undercompensation on the L-band channels, respectively, degrades network performance and reduces the size of the supported ring. The same effect is observed for the OC-192 cases, where EA-modulated transmitters with commercial laser ratings of 1600 ps/nm were used.

V. CONCLUSION

This paper has investigated the feasibility of transparent metropolitan-area WDM optical networks using computer simulation. A multistep simulation methodology has been used effectively for designing the topologies of such networks and engineering their performance. This methodology is based on a combination of wavelength-domain simulations of the entire network followed by time-/frequency-domain simulations on identified worst case paths and efficient budgeting calculations. During the above process, accurate models have been used to describe the most important of the transport-layer impairments that affect the performance of transparent WDM optical networks. Designing such networks and engineering their performance will be a critical task as WDM establishes itself in the present and future rapidly growing metro market.

ACKNOWLEDGMENT

The authors wish to acknowledge the contributions of E. Buckland, D. Q. Chowdhurry, L. Button, J. Bayne, J. Downie, J.-K. Rhee, L. Bhagavatula, V. daSilva, Y. Barberio, and M. Newhouse, all of Corning Inc.

REFERENCES

[1] C. A. Brackett, "Foreword: Is there an emerging consensus on WDM networking?," *J. Lightwave Technol.*, vol. 14, pp. 936–941, June 1996.
[2] The size and growth rate of the Internet, K. G. Coffman and A. Odlyzko. (1998, Oct.). [Online]. Available: www.firstmonday.dk/issues
[3] A. A. M. Saleh and J. M. Simmons, "Architectural principles of optical regional and metropolitan access networks," *J. Lightwave Technol.*, vol. 17, pp. 2431–2448, Dec. 1999.
[4] P. Leisching, H. Bock, A. Richter, C. Glingener, P. Pace, B. Keyworth, J. Philipson, M. Farries, D. Stoll, and G. Fischer, "Architectural principles of optical regional and metropolitan access networks," *IEEE Photon. Technol. Lett.*, vol. 12, pp. 918–920, July 2000.
[5] K.-D. Langer, J. Vathke, G. Walf, U. Broniecki, L. Dembeck, G. Eilenberger, R.-P. Baraun, A. Gladisch, S. Szuppa, H. Bock, P. Leisching, A. Richter, and W. Grupp, "Transparent interconnection of multi-vendor metropolitan sub-networks," in *Proc. IEE ECOC Eur. Conf. Opt. Commun.*, Munich, Germany, Sept. 2000, pp. 4.87–4.88.
[6] T. Pfeiffer, H. Schmuck, B. Deppisch, M. Witte, and J. Kissing, "TDM/CDM/WDM approach for metro networks with 200 optical channels," in *Proc. IEE ECOC Eur. Conf. Opt. Commun.*, Munich, Germany, Sept. 2000, pp. 3.71–3.72.
[7] M. Morin, J. Chauvin, D. H. B. Hoa, L. Berthelon, and O. Rofidal, "Pan-European lightwave core and access network (ACTS pelican project)," in *Proc. IEE ECOC Eur. Conf. Opt. Commun.*, Munich, Germany, Sept. 2000, pp. 4.85–4.86.
[8] K. Y.-Jarkko, S. Tammela, T. Niemi, and A. Tervonen, "Scalability of a metropolitan multi-fiber bidirectional WDM ring network," in *Proc. IEE ECOC Eur. Conf. Opt. Commun.*, Munich, Germany, Sept. 2000, pp. 3.81–3.82.
[9] I. M. White, D. Wonglumsom, K. Shrikhande, S. M. Gemelos, M. S. Rogge, and L. G. Kazovsky, "The architecture of HORNET: A packet-over-WDM multiple-access optical metropolitan area ring network," *Comput. Networks*, vol. 32, pp. 587–598, Sept. 2000.
[10] I. Tomkos, D. Q. Chowdhurry, J. Conradi, D. Culverhouse, K. Ennser, C. Giroux, B. Hallock, T. Kennedy, A. Kruse, S. Kumar, N. Lascar, I. Roudas, M. Sharma, R. S. Vodhanel, and C.-C. Wang, "Demonstration of negative dispersion fibers for DWDM metropolitan area networks," *IEEE J. Select. Topics Quantum Electron.*, vol. 7, pp. 439–460, May/June 2001.
[11] C.-C. Wang, I. Roudas, I. Tomkos, M. Sharma, and R. S. Vodhanel, "Negative dispersion fibers for uncompensated metropolitan networks," in *Proc. IEE ECOC Eur. Conf. Opt. Commun.*, Munich, Germany, Sept. 2000, pp. 381–382.
[12] J. A. J. Fells, M. A. Gibbon, I. H. White, G. H. B. Thompson, R. V. Penty, C. J. Armistead, E. M. Kimber, D. J. Moule, and E. J. Thrush, "Transmission beyond the dispersion limit using a negative chirp electroabsorption modulator," *Electron. Lett.*, vol. 30, pp. 1168–1169, Aug. 1994.
[13] R. W. Tkach, E. L. Goldstein, J. A. Nagel, and J. L. Strand, "Fundamental limits of optical transparency," in *Proc. IEEE/OSA Optical Fiber Commun. Conf.*, San Jose, CA, Feb. 1998, pp. 161–162. paper WJ1.
[14] M. C. Jeruchim, P. Balaban, and K. S. Shanmugam, *Simulation of Communication Systems*. New York: Plenum, 1992.
[15] I. Roudas, N. Antoniades, D. H. Richards, R. E. Wagner, J. L. Jackel, S. F. Habiby, T. E. Stern, and A. F. Elrefaie, "Wavelength-domain simulation of multiwavelength optical networks," *IEEE J. Select. Topics Quantum Electron.*, vol. 6, pp. 348–362, Mar./Apr. 2000.
[16] A. V. Oppenheim and R. W. Schafer, *Discrete-Time Signal Processing*. Englewood Cliffs, NJ: Prentice-Hall, 1989.
[17] L. Kazovsky, S. Benedetto, and A. Willner, *Optical Fiber Communication Systems*. Reading, MA: Artech House, 1996.
[18] N. Antoniades, I. Roudas, R. E. Wagner, J. L. Jackel, and T. E. Stern, "Crosstalk performance of a wavelength selective cross-connect mesh topology," in *Proc. IEEE/OSA Optical Fiber Commun. Conf.*, San Jose, CA, Feb. 1998. paper TuJ4.
[19] I. Roudas, D. H. Richards, N. Antoniades, J. Jackel, and R. E. Wagner, "Efficient erbium-doped fiber modeling for simulation of multiwavelength optical networks," *Opt. Fiber Technol.*, vol. 5, pp. 363–389, Oct. 1999.
[20] N. S. Bergano, F. W. Kerfoot, and C. R. Davidson, "Margin measurements in optical amplifier systems," *IEEE Photon. Technol. Lett.*, vol. 5, pp. 304–306, Mar. 1993.
[21] G. P. Agrawal, *Fiber-Optic Communication Systems*. New York: Wiley, 1997.
[22] N. Antoniades, M. Yadlowsky, and V. L. daSilva, "Computer simulation of a metro WDM interconnected ring network," *IEEE Photon. Technol. Lett.*, vol. 12, pp. 1576–1578, Nov. 2000.
[23] A. R. Chraplyvy, J. A. Nagel, and R. W. Tkach, "Equalization in amplified WDM lightwave transmission systems," *IEEE Photon. Technol. Lett.*, vol. 4, pp. 920–922, Aug. 1992.
[24] A. F. Elrefaie, E. L. Goldstein, S. Zaidi, and N. Jackman, "Fiber-amplifier cascades with gain equalization in multiwavelength unidirectional inter-office ring networks," *IEEE Photon. Technol. Lett.*, vol. 5, pp. 1026–1028, Sept. 1993.
[25] N. Antoniades, A. Boskovic, J.-K. Rhee, J. Downie, D. Pastel, I. Tomkos, I. Roudas, N. Madamopoulos, and M. Yadlowsky, "Engineering the performance of DWDM metro networks," in *Proc. NFOEC National Fiber Optics Engineering Conf.*, Denver, CO, Sept. 2000, pp. 204–211.
[26] A. Ehrhardt, C. Caspar, H.-M. Foisel, B. Strebel, and C. Weinert, "8×2.5 Gbit/s 2340 km transmission experiments over a replica of the Berlin-Darmstadt field transmission line," in *Proc. IEE ECOC Eur. Conf. Opt. Commun.*, Madrid, Spain, Sept. 1998, pp. 277–278.
[27] K. Hinton and T. Stephens, "Modeling high-speed optical transmission systems," *IEEE J. Select. Areas Commun.*, vol. 11, pp. 380–392, 1993.
[28] P. J. Corvini and T. L. Koch, "Computer simulation of high bit rate optical fiber transmission using single frequency lasers," *J. Lightwave Technol.*, vol. 5, pp. 1591–1595, Nov. 1987.
[29]
[30] A. F. Elrefaie, R. E. Wagner, D. A. Atlas, and D. G. Daut, "Chromatic dispersion limitations in coherent lightwave transmission systems," *J. Lightwave Technol.*, vol. 6, pp. 704–709, May 1988.
[31] R. A. Linke, "Modulation induced transient chirping in single frequency lasers," *IEEE J. Select. Topics Quantum Electron.*, vol. QE-21, pp. 593–597, June 1985.
[32] B. W. Hakki, "Evaluation of transmission characteristics of chirped DFB lasers in dispersive optical fiber," *J. Lightwave Technol.*, vol. 10, pp. 964–970, July 1992.
[33] D. Q. Chowdhurry, E. F. Murphy, E. J. Barens, L. H. Jackson, and J. Cattetow, "Measurement of dispersion-compensating module polarization-mode dispersion statistics," in *Proc. IEEE/OSA Optical Fiber Commun. Conf.*, San Jose, CA, Feb. 1997, pp. 260–261.
[34] *Standards References (Draft)*, 2000.
[35] D. Q. Chowdhurry, L. Bhagavatula, L. Button, P. Wigley, and C. Sutton, "Statistical impact of EDFA polarization mode dispersion on long-haul optical systems," in *Proc. IEE ECOC Eur. Conf. Opt. Commun.*, Munich, Germany, Sept. 2000, pp. 147–148.
[36] D. Wang and C. R. Menyuk, "Nonlinear evolution of the polarization states in WDM channels," in *Proc. IEEE/OSA Optical Fiber Commun. Conf.*, San Jose, CA, Feb. 1998.
[37] C. R. Menyuk, D. Wang, and A. N. Pilipetskii, "Repolarizations of polarization-scrambled optical signals due to polarization dependent loss," *IEEE Photon. Technol. Lett.*, vol. 9, pp. 1247–1249, Feb. 1997.
[38] E. L. Goldstein, L. Eskildsen, and A. F. Elrefaie, "Performance implications of component crosstalk in transparent lightwave networks," *IEEE Photon. Technol. Lett.*, vol. 6, pp. 657–660, May 1994.
[39] E. L. Goldstein and L. Eskildsen, "Scaling limitations in transparent optical networks due to low-level crosstalk," *IEEE Photon. Technol. Lett.*, vol. 7, pp. 93–94, Jan. 1995.
[40] D. J. Blumenthal, P. Granestrand, and L. Thylen, "BER floors due to heterodyne coherent crosstalk in space photonic switches for WDM networks," *IEEE Photon. Technol. Lett.*, vol. 8, pp. 284–286, Feb. 1996.
[41] J. Zhou, R. Cadeddu, E. Casaccia, C. Cavazzoni, and M. J. O'Mahony, "Crosstalk in multiwavelength optical cross-connect networks," *J. Lightwave Technol.*, vol. 14, pp. 1423–1435, June 1996.
[42] K.-P. Ho, "Analysis of homodyne crosstalk in optical networks using gram-charlier series," *J. Lightwave Technol.*, vol. 17, pp. 149–154, Feb. 1999.

[43] P. J. Legg, M. Tur, and I. Andonovic, "Solution paths to limit interferometric noise induced performance degradation in ASK direct detection lightwave networks," *J. Lightwave Technol.*, vol. 14, pp. 1943–1954, Sept. 1996.

[44] X. Jiang and I. Roudas, "Asymmetric probability density function of a signal with interferometric crosstalk," *IEEE Photon. Technol. Lett.*, vol. 13, pp. 160–162, Feb. 2001, to be published.

[45] K. Feher, *Advance Digital Communications Systems and Signal Processing Techniques*. Englewood Cliffs, NJ: Prentice-Hall, 1997.

[46] E. Lichtman, "Limitations imposed by polarization-dependent gain and loss on all-optical ultralong communication systems," *J. Lightwave Technol.*, vol. 13, pp. 906–913, May 1995.

[47] D. Q. Chowdhurry, L. Bhagavatula, L. Button, P. Wigley, and C. Sutton, "PDL induced gain ripple statistics in EDFA," *Proc. IEE ECOC Eur. Conf. Opt. Commun.*, pp. 3.81–3.82, Sept. 1999.

[48] I. Roudas, N. Antoniades, T. Otani, T. E. Stern, R. E. Wagner, D. Q. Chowdhurry, and L. D. Garrett, "Accurate modeling of optical multiplexer/demultiplexer concatenation in multiwavelength optical networks," *J. Lightwave Technol.*, submitted for publication.

[49] C. Caspar, H.-M. Foisel, C. V. Helmolt, B. Strebel, and Y. Sugaya, "Comparison of the cascadability performance of different types of commercially available wavelength (de)multiplexers," in *Proc. IEE ECOC Eur. Conf. Opt. Commun.*, Edinburgh, Scotland, Sept. 1997, pp. 3.91–3.94.

[50] N. N. Khrais, A. F. Elrefaie, R. E. Wagner, and S. Ahmed, "Performance degradation of multiwavelength optical networks due to laser and (de)multiplexer misalignments," *IEEE Photon. Technol. Lett.*, vol. 7, pp. 1348–1350, Nov. 1995.

[51] ——, "Performance of cascaded misaligned optical (de)multiplexers in multiwavelength optical networks," *IEEE Photon. Technol. Lett.*, vol. 8, pp. 1073–1075, Aug. 1996.

[52] T. Otani, N. Antoniades, I. Roudas, and T. E. Stern, "Cascadability of passband-flattened arrayed waveguide grating filters in WDM optical networks," *IEEE Photon. Technol. Lett.*, vol. 11, pp. 1414–1416, Nov. 1999.

[53] I. Tomkos, R. Hesse, N. Antoniades, and A. Boskovic, "Impact of filter concatenation on the performance of metropolitan area optical networks utilizing directly modulated lasers," in *IEEE/OSA Optical Fiber Commun. Conf. Dig.*, Anaheim, CA, Mar. 2001.

[54] I. Tomkos, I. Roudas, A. Boskovic, R. Hesse, N. Antoniades, and R. S. Vodhanel, "Measurements of laser rate equation parameters for representative simulations of 2.5 Gb/s metro area IM/DD transmission systems and networks," in *Proc. IEEE/LEOS Annual Meeting*, San Juan, Puerto Rico, Nov. 2000, pp. 692–693.

[55] A. Dwivedi and R. E. Wagner, "Traffic model for USA long-distance optical network," in *Proc. IEEE/OSA Optical Fiber Commun. Conf.*, Baltimore, MD, Feb. 2000, pp. 156–158. paper TuK11.

Neophytos Antoniades (M'98) received the B.S., M.S., M.Phil., and Ph.D. degrees in electrical engineering from Columbia University, New York, in 1992, 1993, 1996, and 1998, respectively.

His Ph.D. work focused on modeling of optical components, WDM communication systems, and networks. During 1994 to 1998, he was a Research Associate with Bellcore, Red Bank, NJ, and was involved in both the Optical Networks Technology Consortium (ONTC) and the Multi-Wavelength Optical Networking (MONET) programs. Within MONET, he was part of a team that designed and developed a wavelength-domain computer simulator for studying performance impairments in WDM optical networks. In 1998, he joined Corning Inc. as a Senior Research Scientist at the Photonic Research & Test Center, Somerset, NJ, where he worked on the design and support of current as well as next-generation products. He is now a Supervisor doing research on advanced fiber-optic systems and networks to support development of telecommunication fiber and optical network elements. Among his interests are modeling transport-layer impairments in WDM networks and optical networking in general. He has published extensively in all leading journals and conferences. He currently holds two patents in the field of fiber optics with three others pending.

Dr. Antoniades is a member of IEEE-LEOS organizations and a member of the LEOS Annual Conference Committee on Optical Networks and Systems. He has also served as a Reviewer for the IEEE/OSA JOURNAL OF LIGHTWAVE TECHNOLOGY and IEEE PHOTONICS TECHNOLOGY LETTERS.

Aleksandra Boskovic received the B.S. and M.S. degrees in physics from the Pontifical Catholic University of Rio de Janeiro, Brazil, in 1988 and 1991, respectively, and the Ph.D. degree in physics from the University of London, Imperial College, U.K., in 1996.

She joined the Science and Technology Division, Corning Inc., Corning, NY, as a Senior Scientist in 1997 and since then has worked on optical fiber and components transmission system impairments and optical networking in general. She is currently a Manager at Corning Inc., leading a group in Optical Network Performance.

Dr. Boskovic is a member of the Optical Society of America.

Ioannis Tomkos received the B.Sc. degree in physics from the University of Patras, Greece, and the M.Sc. degree in telecommunications engineering and Ph.D. degree in optical telecommunications from the University of Athens, Greece.

He is a Senior Research Scientist with Corning Inc., Corning, NY. Previously, he was a Research Fellow at the Optical Communications Laboratory of the University of Athens, Greece, where he participated in several national and European research projects (e.g., ACTS, COST). His recent research has focused on transport issues related to optical networks. In the past, he researched novel wavelength conversion technologies based on nonlinear effects in semiconductor optical amplifiers and fibers. He is an author or coauthor of about 50 papers, published in international journals and conference proceedings. He is currently leading efforts related with transport performance and technology trends.

Dr. Tomkos has been awarded for his research accomplishments from several engineering societies, including IEEE and SPIE.

Nicholas Madamopoulos (S'95–M'99) was born in Athens, Greece, in 1970. He received the B.S. degree in physics (with honors) from the University of Patra, Greece, in 1993 and the M.S. and Ph.D. degrees in optical science and engineering from the School of Optics, Center for Research and Education in Optics and Lasers (CREOL), University of Central Florida, Orlando, in 1996 and 1998, respectively.

After receiving the B.S. degree, he joined the Applied Optics and Optical Processing Laboratory of the Institute of Electronic Structures and Lasers, Foundation for Research and Technology-Hellas, Heraklion, Greece, as a Research Fellow. There, he did research on dynamic diffraction at the near infrared and excimer laser micromachining for computer-generated holograms and microoptic diffractive elements. In August 1994, he received a Graduate Optics Fellowship from CREOL. His Ph.D. specialization was in photonic information processing systems, where he introduced novel photonic delay lines for phased array antenna applications. He was a Graduate Research Fellow at the Photonic Information Processing Systems Laboratory at CREOL. He also joined Light Bytes, Inc., where he helped establish the company and won the company's first SBIR, completing Phase I with success. In summer 1999, he joined the Network Architecture and Equipment Department, Corning, Inc., Corning, NY, where he concentrated on modeling the optical performance of the physical layer of optical network architectures. In fall 2000, he joined the Corning Photonics Research and Test Center facility in Somerset, NJ, where he is mostly involved with experiments. His research interests are optical networking and transport-layer performance.

Dr. Madamopoulos is a member of IEEE-LEOS and the Optical Society of America (OSA). He received a New Focus Student Essay Prize in 1996, the SPIE Educational Scholarship in Optical Engineering in 1997, a Graduate Merit Fellowship award in 1998, and a New Focus/OSA Student Award in 1998. He was one of the Founding Members of the first IEEE-LEOS Student chapter and served as Treasurer and President for several years.

Mirim Lee (M'00) received the B.S. and M.S. degrees in physics from Seoul National University, Seoul, Korea, and the Ph.D. degree in condensed matter physics from the University of Florida, Gainesville, in 1996.

She was a Postdoctoral Fellow at the University of Houston, Houston, TX, until 1998. Currently, she is a Research Scientist at Corning Inc., Corning, NY, focusing on modeling transmission system impairments.

Ioannis Roudas was born in Athens, Greece, in 1966. He received the Diploma in physics and the Certificate of Electronics and Radio-Engineering from the University of Athens, Greece, in 1988 and 1990, respectively, and the M.S. and Ph.D. degrees from ENST, Paris, France, in 1991 and 1995, respectively.

His Ph.D. dissertation concerned modeling and optimal design of coherent optical communication systems. During 1995–1998, he was with the Optical Networking Research Department, Bell Communications Research, Red Bank, NJ, where he was involved in the Multiwavelength Optical Networking (MONET) project. His research mainly focused on the development of an efficient computer representation of the MONET optical transport layer. In parallel, during the fall semesters of 1997 and 1998, he taught the graduate course "Lightwave Systems" as an Adjunct Professor of electrical engineering at Columbia University, New York. Since 1999, he has been a Senior Research Scientist in the Photonic Research and Test Center, Corning Inc., Somerset, NJ. His current research concerns modeling of transmission effects in high-data-rate optical communications systems and networks.

Dr. Roudas is a Reviewer for the IEEE/OSA JOURNAL OF LIGHTWAVE TECHNOLOGY and the IEEE PHOTONICS TECHNOLOGY LETTERS.

David Pastel received the B.S. and M.Eng. degrees in engineering physics and the Ph.D. degree in electrical engineering from Cornell University, Ithaca, NY, in 1990, 1991, and 1999, respectively.

He has been with Corning Inc., Corning, NY, since 1991. From 1991 to 1999, he invented, developed, and installed measurements systems for the fiber-optic manufacturing process for the Telecommunications Products division. For the last two years, he has been with Applied Research in the Optical Network Devices Division working on new product development.

Manish Sharma was born in Rohtak, India, on January 29, 1972. He received the M.Eng. degree in electrical and electronic engineering from University College London, London, U.K., in 1990 and the Ph.D. degree in electronic engineering from Sophia University, Tokyo, Japan, in 1998.

He joined Toshiba Corporation, Tokyo, in 1990, where he was engaged in the research and development of long-haul optical communication systems and wavelength-division multiplexing techniques. In 1998, he joined Corning Inc., Corning, NY, and has been involved in the research and development of optical networking systems and enabling technologies.

Michael J. Yadlowsky received the B.S. degree from the University of Virginia, Charlottesville, and the M.S. and Ph.D. degrees from the University of Colorado, Boulder, all in electrical engineering.

He joined the Science and Technology Division, Corning Inc., Corning, NY, as a Senior Research Scientist in 1995 and worked on rare-earth-doped fiber amplifiers, optical networking, and optical fiber transmission system impairments. He is currently a Manager in Corning Inc.'s Optical Networking Devices division. From 1993 to 1995, he was a National Research Council Associate at the National Institutes of Health, where he conducted research on optical reflectometry techniques for biomedical applications.

Dr. Yadlowsky is a member of the Optical Society of America and Sigma Xi.